ICAS-84-1.5.1 STEADY AND UNSTEADY PRESSURE DISTRIBUTIONS ON A NACA 0012 PROFILE IN SEPARATED TRANSONIC FLOW

H. Triebstein
Institute of Aeroelasticity, DFVLR-AVA
Göttingen, W. Germany

Abstract

Steady and unsteady aerodynamic data were measured on a two-dimensional model with an airfoil of 12% thickness mounted in the Transonic Windtunnel of the DFVLR in Göttingen. The profile was oscillated in pitch about its c/4 axis to generate the unsteady aerodynamic pressure data. The purpose of the windtunnel test was primarily to measure data for use in the development and assessment of transonic analytical codes and to show the dependence of aerodynamic responses on the following parameters: Mach number (0.5 to 1.0), reduced frequency (0.02 to 0.12) angle of attack (0 to 9°) and oscillation amplitude (0.5 to 2.5°). Emphasis is also placed on the nonlinearities which actually occur and which are peculiar to higher angles of attack. Steady and unsteady calculation results agreed fairly well with the measured data.

Nomenclature

x,y,z	Cartesian coordinates, see Fig.1
c	wing chord
V	steady freestream velocity
α	angle of attack
Re	Reynolds number (= $Vc\rho/\mu$)
μ	dynamic air viscosity
ρ	air density
M	freestream Mach number (= V/a)
a	sonic speed
f	oscillation frequency
ω	angular frequency (= $2\pi f$)
ω^*	reduced frequency (= $\omega c/2V$)
$\Delta\alpha$	pitching oscillation amplitude
$\overline{\Delta\alpha}$	pitching oscillation amplitude in radian measure
c_p	nondimensional pressure coefficient (= $(\bar{p} - p_0)/q$)
$\bar{p}$	steady pressure
p	unsteady pressure
p_0	stagnation pressure
q	dynamic pressure (= $\rho V^2/2$)
c_p', c_p''	real and imaginary parts of the nondimensional and standardized pressure coefficient (= $p/(q\cdot\overline{\Delta\alpha})$)

Introduction

In addition to information on the elastic behavior of a structure, it is necessary that the unsteady aerodynamic forces acting on the structure are known as well in order to guarantee the aeroelastic stability of all kinds of aircraft. Knowledge of these unsteady aerodynamic forces requires in turn an understanding of the steady forces. At the present stage of aircraft development, it is imperative that particular attention be drawn to the realm of transonic flow and the separation phenomena which occur therein. Special interest is focussed on supercritical wings and control surfaces of active control systems.

In the theoretical sector, modern computers have facilitated gradual access to the transonic flow range. Correspondingly, this paper is devoted to experimental determination of the steady and unsteady pressure distributions on a NACA 0012 profile, in order to develop ideas on how to improve present theoretical approaches and calculation methods. The NACA 0012 profile was chosen for this investigation because it appears on the list of the Working Group of the AGARD Structures and Materials Panel.

Above all, the measured data are meant to demonstrate the dependence of the aerodynamic responses on known parameters. Moreover, the nonlinearities which actually occur are clearly shown, because in most of the known experiments no attempt has been made to measure any of the higher harmonics although large nonlinearities were known to occur at a shockwave. Most of the sources dealing with these problems are given in Ref.[1]. The measurements were performed in March of 1982 in the Transonic Windtunnel of the DFVLR in Göttingen.

Windtunnel

The Transonic Windtunnel of the DFVLR in Göttingen, W.Germany, is a closed-circuit, continuous-flow tunnel which has a 1m x 1m test section with perforated walls. Mach number and the dynamic pressure, and thus the Reynolds number, can be varied simultaneously or independently, with air as test medium.

Test setup and wing configuration

A schematic diagram of the test setup is shown in Figure 1. The test model is supported on either side by ball bearings outside the perforated windtunnel walls. Excitation of the model to pitch oscillations about its c/4 axis is achieved by means of a hydraulic rotation cylinder, the pump of which is located outside the windtunnel. A coupling mechanism provides rigid connection in radial direction while relieving the hydraulic cylinder in axial

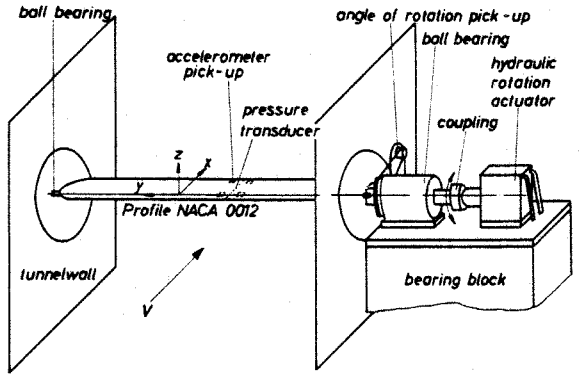

Figure 1: Test setup.

direction. An angle of rotation pickup is mounted outside the windtunnel wall, allowing the angle of attack as well as the pitch oscillation amplitude to be adjusted and monitored.

The wing instrumentation consists of 30 differential pressure transducers (Kulites, ± 5 psi), four accelerometers and two angle of rotation pickups. The transducers are mounted in spanwise direction along the middle axis of the model to measure both static and dynamic pressures. The pressure transducers on the upper side of the model are staggered for purposes of rigidity and in order to save space. The 21 pickups on the upper surface are located at

(x/c)100 = 0, 1.5, 5, 10, 15, 20, 25, 30, 35, 40, 45, 50, 55, 60, 65, 70, 75, 80, 85, 90, 95

and the 9 pickups on the lower side at

(x/c)100 = 10, 20, 30, 40, 50, 60, 70, 80, 90.

The task of the four accelerometers is to control the stiffness of the model.

The wing has a rectangular planform with a chord of 0.2 m and a span of 1.0 m, reaching from wall to wall. The airfoil has the theoretical coordinates of the NACA 0012 profile: the actual coordinates are given in Table 1. The model itself is composed of two halves; the entire leading and trailing edges are added to the upper surface of the model. In order that the model be kept reasonably lightweight, and thus have a higher natural frequency, the model shell is quite thin and is constructed of a light metal alloy. The model supports are made of steel. Fiberglass-reinforced ribs inside the model provide extra rigidity. Ground vibration tests have shown that the lowest natural bending frequency for this wing configuration is over 50 Hz.

x/c	$-(z_L/c)100$	$(z_U/c)100$
0.0000	0.0117	0.0117
0.0025	0.8623	0.8736
0.0050	1.1937	1.2218
0.0100	1.6884	1.7138
0.0250	2.6364	2.6320
0.0500	3.5791	3.5684
0.0700	4.1147	4.1017
0.1000	4.7159	4.7028
0.1600	5.4722	5.4635
0.2000	5.7625	5.7609
0.2600	5.9804	5.9917
0.3000	6.0223	6.0344
0.3625	5.9511	5.9651
0.4200	5.7655	5.7680
0.4600	5.5696	5.5671
0.5000	5.3302	5.3304
0.6000	4.5950	4.5984
0.6600	4.0717	4.0696
0.7000	3.6915	3.6876
0.7600	3.0813	3.0790
0.8000	2.6523	2.6436
0.8600	1.9666	1.9544
0.9000	1.4735	1.4685
0.9600	0.6956	0.7013
1.0000	0.1260	0.1260

Table 1: Actual coordinates.

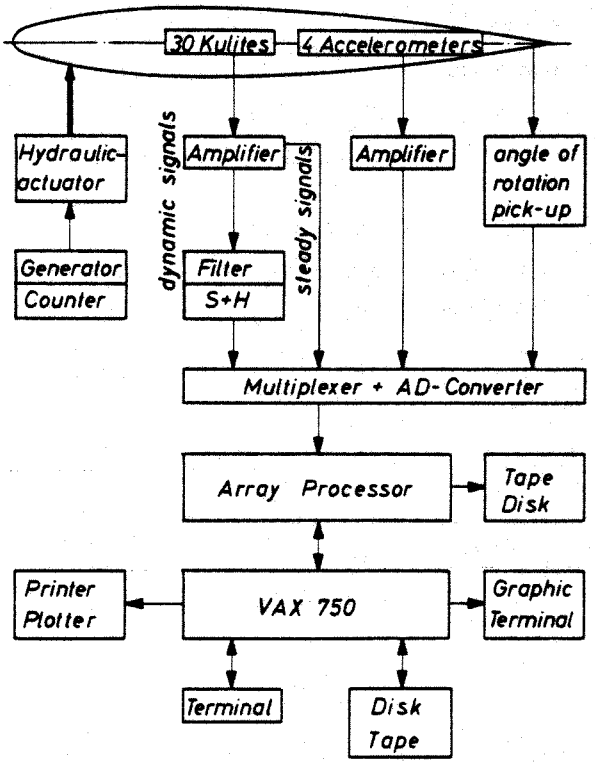

Figure 2: Block-circuit diagram of the electronic measuring equipment.

Electronic data recording and processing

The electronic measuring equipment, which will be described in some detail in this section, is illustrated by the block circuit diagram in Figure 2. The portable real-time data acquisition system is designed for aeroelastic research and testing when large amounts of dynamic data are required over a wide frequency range.

The scope of the present investigation included measuring the following quantities:

a) Steady pressure distributions on the model using differential pressure transducers located on the wing;

b) Unsteady pressure distributions on the model using the same differential pressure transducers;

c) Angle of attack and oscillation amplitudes of the pitching motions by means of angle of rotation pickups;

d) Control of the rigidity of the model by means of acceleration pickups.

A frequency generator was used to produces sinusoidal voltages of the desired frequency ω. Using a quartz-controlled frequency counter, this frequency can be measured quite accurately. The amplified alternating voltage is then supplied to the control winding of the hydraulic exciter that induces the model to perform harmonic pitching oscillations.

The voltages of the dynamic pressures are conducted via temperature-compensated amplifiers, low-pass filters, a multiplexer and an AD-converter to the array processor. The unsteady pressures are calculated from transducer time-history data measured at a rate of $(32 \times \omega/2\pi)$ samples per second (max. 400,000 samples per second). A cross spectral analysis of the data is used to determine the harmonic pressure coefficients magnitude and phase or real and imaginary parts in relation to the pitch oscillation of the wing model.

The steady pressures are measured using the same differential pressure transducers as for the unsteady pressures. Ten thousand samples of data at a rate of 1000 samples per second were averaged for each transducer to determine mean values of the pressure coefficients. Data were acquired simultaneously from all transducers. Aeroelastic deformation of the wing profile during the pressure data acquisition process can be controlled by discrete Fourier transforms of time-history data measured by the accelerometers. The real-time data acquisition system is described in detail in Ref.[2].

Measuring procedure

In this test the direct method is applied, i.e. the pressure is measured by in situ pressure transducers. Using temperature-compensated amplifiers developed by the DFVLR in Göttingen, it is possible to measure the steady as well as unsteady pressures with the same transducer simultaneously. The advantage of this method lies in the fact that the costly operation time of the windtunnel is reduced and that the steady and unsteady pressures are measured at the same location. The disadvantage of this method is the high expense of the in situ pressure transducers and the necessary electronic equipment. With careful handling of these small pressure-measuring elements, however, it is possible to use them again so that the initially high expense is justified. It is only possible to measure the steady pressure during oscillation of the model in nonseparated flow without shock (Figure 3).

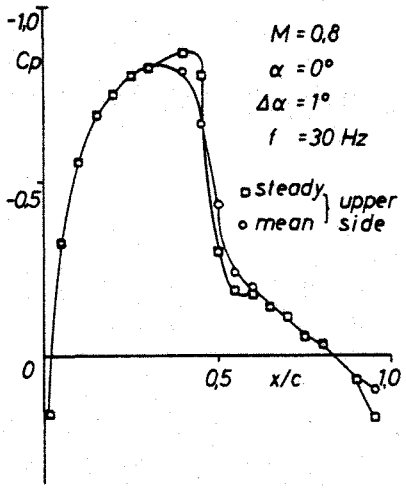

Figure 3: Pressure patterns of the steady and mean pressure.

This picture facilitates a comparison of mean and steady pressures. The differences evident in the realm where shock and separation occur are plain to see. The pressure curve of the mean pressure in the shock region is smoother. By plotting the quotients of mean and steady pressure with respect to the nondimensional profile chord, it becomes clear that the differences of the two pressures in the unseparated flow region are due to measuring inaccuracies (Figure 4). In the shock area, the differences between the two curves are considerable, owing to the smoothness of the mean pressure curve. Differences in the post-shock area are a result of the flow, which tends to separate here or which separates differently

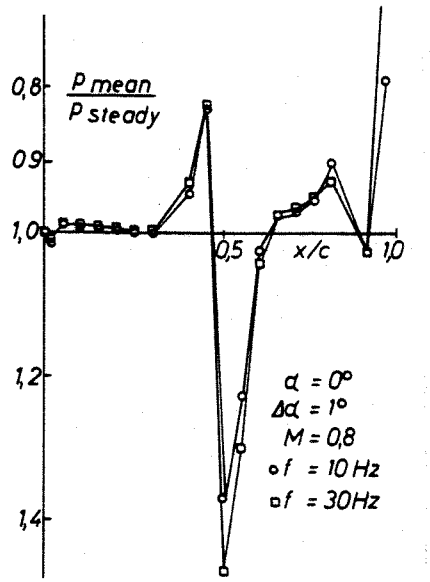

Figure 4: Influence of shock and separation on steady and mean pressure.

according to the various prevailing pressures. One should bear in mind, however, that errors are inherent in the quotient-formation process at small numbers. The results discussed here are valid for various oscillation frequencies, angles of attack, Mach numbers and oscillation amplitudes. In addition, bubbles on the leading edge of the profile caused by the various parameters lead to considerable differences between mean and steady pressure.

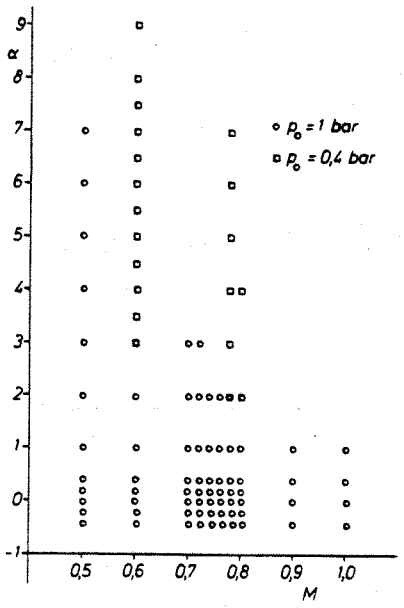

Figure 5: Test runs for measuring steady pressure.

Test program

Steady, mean and unsteady pressures were measured for a large number of test conditions in the Transonic Windtunnel of the DFVLR in Göttingen as illustrated in Figures 5 and 6, which show the angle of attack plotted with respect to Mach number. The stagnation pressure was 1 bar; only in some cases were the measurements made at 0.4 bar. For the unsteady runs, the oscillation frequencies were 10 and 30 Hz. Variations of the oscillation amplitudes ($\Delta\alpha$ = 0.5, 1, 1.5, 2, 2.5°) were made at p_0 = 0.4 bar. Selected results obtained during these tests are presented in this report.

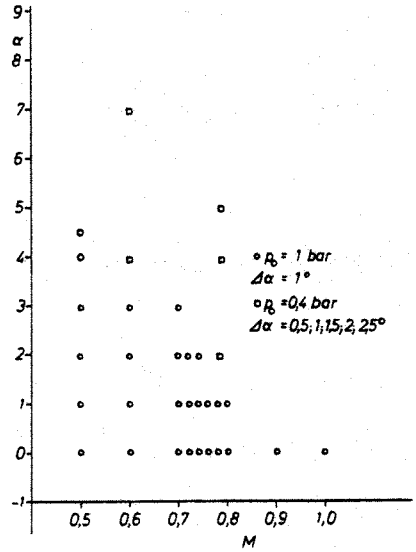

Figure 6: Test runs for measuring the mean and the unsteady pressure.

Test results and discussion

It is widely known that investigations performed in windtunnels of relatively small diameter usually require a correction of the effective angle of attack. A dependence on the resulting lift applied to the test profile cannot be ignored. Compared to supercritical profiles, the correction for the NACA 0012 profile, however, is minor. In the case of the NACA 0012 profile at zero incidence in the Transonic Windtunnel, an angle of attack correction of α = -0.2 to 0.2° is necessary for the Mach number range M = 0.5 to 0.9.

The steady pressures presented here are nondimensionalized by the dynamic pressure. In addition the unsteady values are normalized to the amplitudes and plotted versus the nondimensional wing chord x/c.

The unsteady pressure coefficients are calculated from the recorded time signals. The results are not expressed in terms of phase and amplitude as is often the case, but in terms of real and imaginary parts, i.e. the real part is in-phase with the oscillations and the imaginary part is shifted 90°. The oscillations toward positive angles of attack are positive for the pitching motions about the c/4-axis of the model.

Steady results

As mentioned earlier, the steady as well as the mean pressure distributions are determined, the latter being determined concurrently with the unsteady values. The average steady values in this case serve mainly as input into an unsteady, time-linearized, potential-theoretical Transonic Method[3], which provides the fundamental frequency of the unsteady Δc_p-distribution.

The measurements are taken without transition strip for two different Reynolds numbers. The free transition indicates a λ-shock of the pressure recovery on the wing, which can be confirmed by means of schlieren photography. Noteworthy differences between the results for the two different Reynolds numbers occur only within the range of the greatest negative pressure, Figure 7. Experience with other profiles has shown that it is better to take measurements at the Reynolds numbers reached in this case without a transition strip.

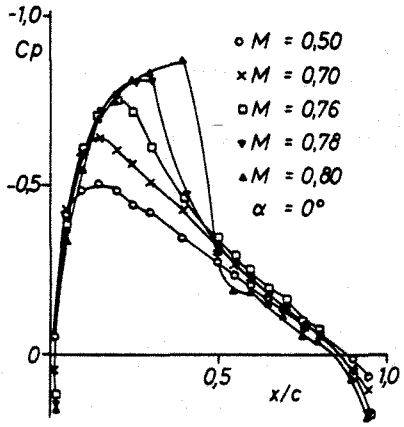

Figure 8: Effects of the Mach number on steady pressure.

Since the parameters Mach number and angle of attack exert a great influence on the unsteady pressure distributions, the effect of these two parameters on steady pressure is analyzed as well. In Figure 8 the nondimensional pressure c_p of the profile's upper side is presented versus the nondimensional profile chord x/c for the entire Mach number range with angle of attack $\alpha = 0°$. These figures show that, in the case of M = 0.76, the critical Mach number is exceeded, although only the shock waves at M = 0.78 and M = 0.8 can be considered intense. In this case, the Reynolds number varies with the Mach number. Figure 9 shows for Mach number 0.78 the influence of the angle of attack on the steady pressure. The location of the shock

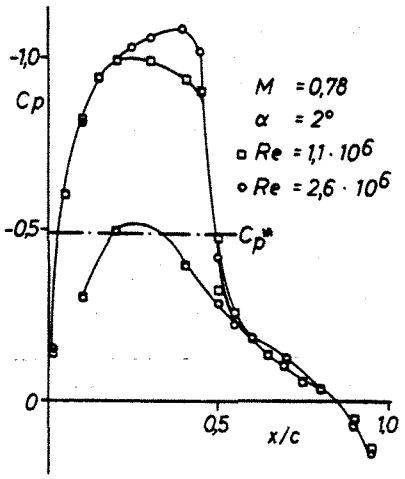

Figure 7: Effects of the Reynolds number on steady pressure.

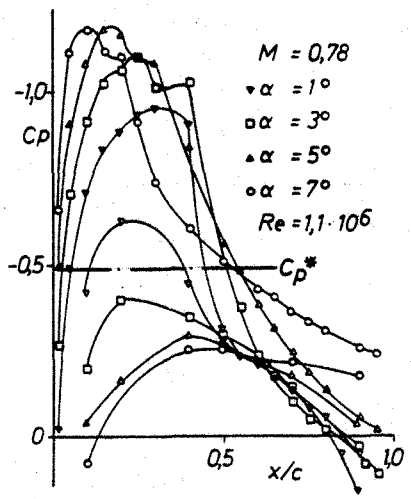

Figure 9: Effects of the angle of attack α on steady pressure.

wave shifts with increasing angle of attack toward the trailing edge of the profile. This process is then reversed after a certain α-value has been exceeded. For angles of attack α = 5° and 7°, it is clear that flow separation is caused by shock.

The advantages of the newly developed supercritical profiles in the realm of transonic flow are indicated in Figure 10. Although the A3 profile (MBB Munich) is not shockfree at M = 0.8, an incomparably high lift coefficient, due especially to the rear-loading region, is evident even at low angles of attack.

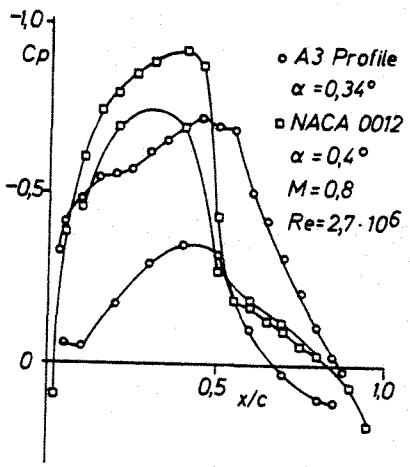

Figure 10: Comparison between the NACA 0012 profile and a supercritical profile.

Unsteady results

The scope of this paper allows only a small part of the measured unsteady pressure distribution to be presented. Results are shown which illustrate the influence of the parameters Mach number, angle of attack, reduced frequency and oscillation amplitude. In addition, the unsteady pressures with regard to the higher harmonic parts are investigated for several particularly significant cases.

Mach number effects. Unsteady pressure distributions on the upper side of the model are shown in Figure 11 for five Mach numbers in the range from 0.5 to 0.9. The mean angle of attack is 0°. The oscillation amplitude is 1° with an oscillation frequency of 30 Hz. Accordingly, the reduced frequency ω* ranges from 0.108 to 0.063 for Mach numbers M = 0.5 to 0.9.

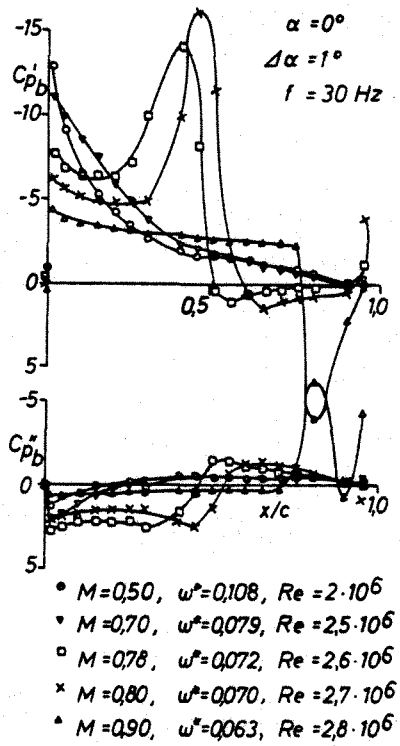

Figure 11: Effects of Mach number on unsteady pressure distribution on the upper side of the model.

At M = 0.7, the pressure curve behaves in the manner typical for subsonic flow and the critical pressure is not exceeded in this case. At M = 0.78 the critical pressure is markedly exceeded, forming a pressure peak which declines with the occurrence of shock. The pressure peak shifts rapidly with increasing Mach number toward the trailing edge and the real part changes its sign at M = 0.9 due to the flow separation which occurs here. The sign of the imaginary part changes with the location of the shock. With regard to the phase data, the pressures ahead of the shock lag behind the motion and those behind the shock precede the motion.

Mean angle of attack effects. The unsteady pressure distributions on the upper side are shown in Figure 12 at angles of attack 0, 1, 2, 4 and 5°. The Mach number is M = 0.78 with oscillation amplitude Δα = 1°, oscillation frequency f = 30 Hz and thus ω* = 0.073. For angles of attack α = 2, 4 and 5°, the measurements are taken at reduced stagnation pressure, which leads to various Reynolds numbers. The shock location shifts with increasing angle of attack toward the trailing edge of the profile, until flow separation occurs at α = 4 and 5° and thus the sign of the real part changes. After flow separation has occurred, the shock location appears stable as shock-induced separation at

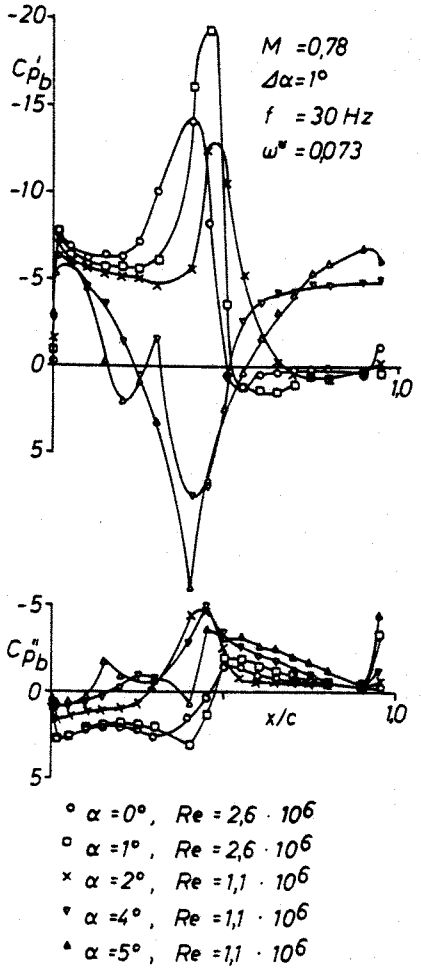

Figure 12: Effects of mean angle of attack on unsteady pressure distribution on the upper side of the model.

α = 4 and 5° continues up to the trailing edge. The influence on the mean pressure due to separation is considerably weaker than that on the unsteady pressure. The first discontinuity of the real-part pressure curve for α = 4° indicates the presense of a λ-shock and the magnitude of the oscillation amplitude is instrumental in determining the form of the induced λ-shock. The intensity of the shock strongly influences the extent of the pressure distribution in front of the shock.

Oscillation frequency effects. Figure 13 shows the unsteady pressure distribution for two frequencies (10 and 30 Hz), Mach number M = 0.78, oscillation amplitude Δα = 1° and two angles of attack α = 0 and 5°. The shock location is not altered by the oscillation frequencies and the real part of the pressure amplitude is only slightly affected. The phase, however, is shifted considerably over the imaginary part.

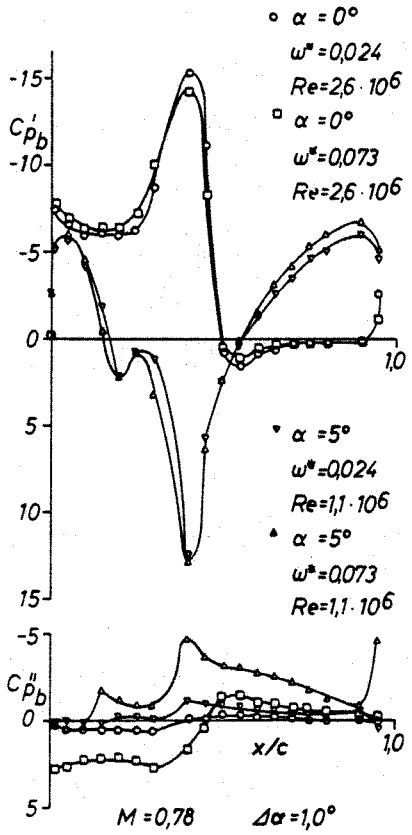

Figure 13: Effects of oscillation frequency on unsteady pressure distribution on the upper side of the model.

Oscillation amplitude effects. Figures 14, 15 and 16 present the unsteady pressure distributions at two Mach numbers and high angles of attack for various oscillation amplitudes. Since the unsteady pressures are normalized to the oscillation amplitudes, the pressure curves are expected to coincide, assuming linear behavior. Plotted results show, however, that a slight nonlinear dependence of the unsteady pressures caused by the oscillation amplitudes occurs already in the region of low supersonic velocities as well as in the recompression area of the flow (Fig.14). More intense nonlinearities occur when shock waves develop due to recompression, which completely vanish when the flow reattaches (Fig.15). If the flow following a shock wave does not reattach, the nonlinearities do not vanish before the profile edge is reached (Fig.16). This figure clearly shows the influence of the oscillation amplitude on the pressure curve at the site of the oblique shock of the λ-shock.

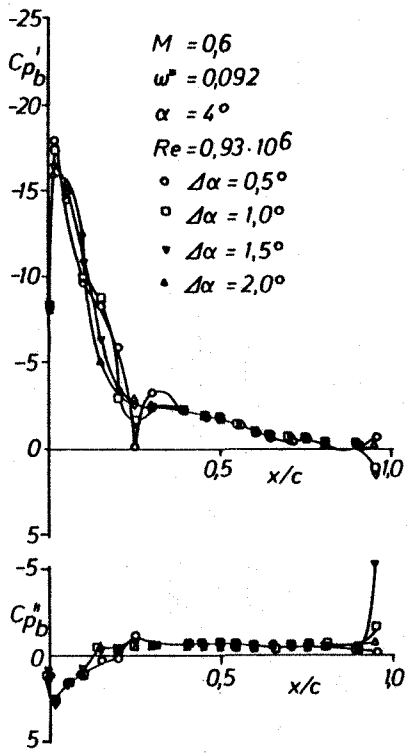

Figure 14: Effects of oscillation amplitude on the unsteady pressure distribution; M = 0.6, α = 4°.

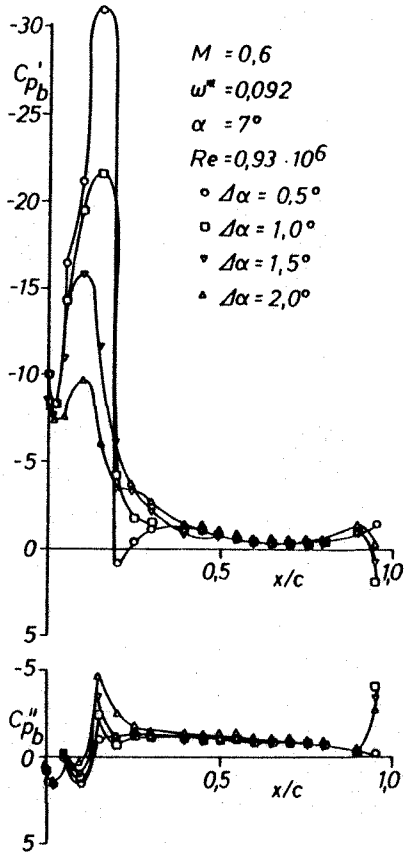

Figure 15: Effects of oscillation amplitude on the unsteady pressure distribution; M = 0.6, α = 4°.

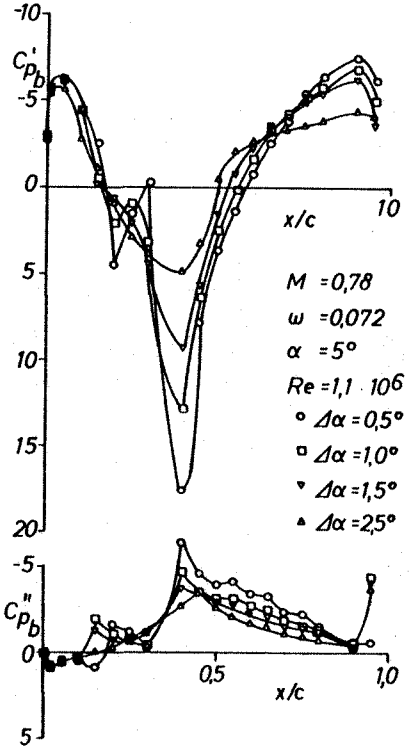

Figure 16: Effects of oscillation amplitude on the unsteady pressure distribution; M = 0.78, α = 5°.

Higher harmonic parts of unsteady pressure

Admittedly, a somewhat unconventional format for presenting the higher harmonic parts of unsteady pressure was purposely chosen in order for the figures to accommodate as much information as possible. The amplitude values of each higher harmonic part measured are taken from the plotted power spectrum and recorded in addition to the previously determined first harmonic part (Figures 17a, b, 18a, b, 19a and b). In this process, the highest value is set at 1 and the lower values are given as a percentage thereof. Information on the phase term of these parts, however, is thus lost.

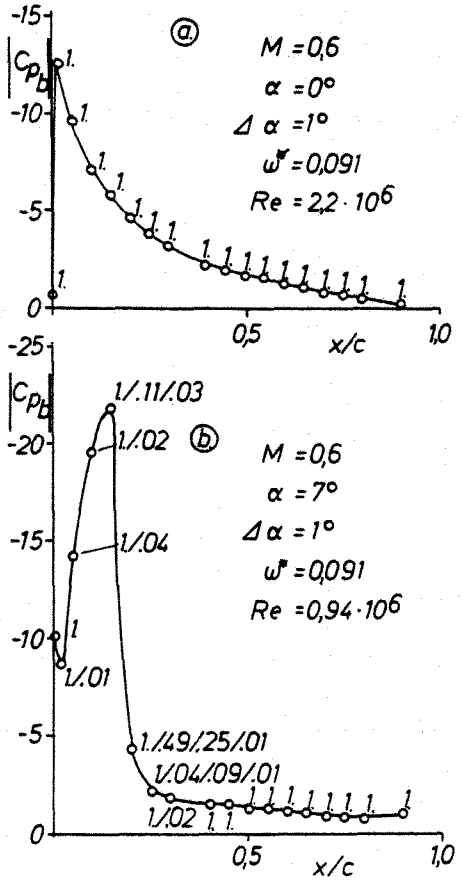

Figure 17a,b: Magnitude data of the first harmonic and of the higher harmonic unsteady pressure, M = 0.6.

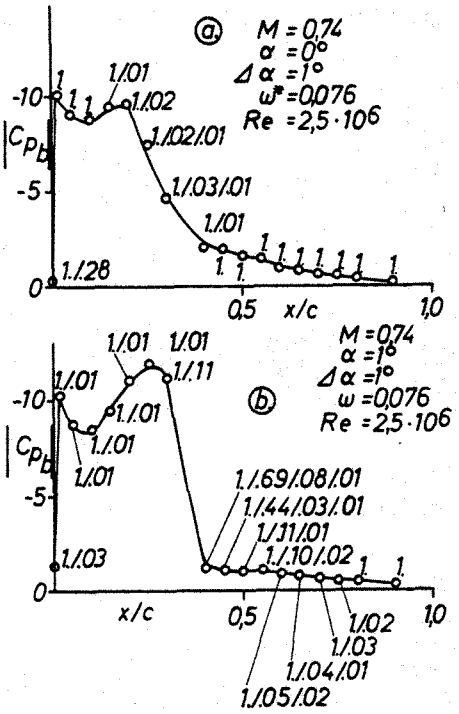

Figure 18a,b: Magnitude data of the first harmonic and of the higher harmonic unsteady pressure, M = 0.74.

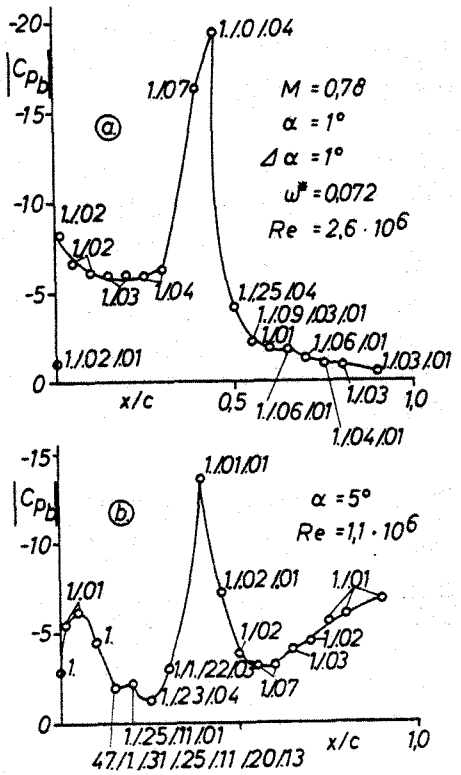

Figure 19a,b: Magnitude data of the first harmonic and of the higher harmonic unsteady pressure, M = 0.78.

The unsteady pressure amplitudes appear in Fig.17a for M = 0.6 and, $\alpha = 0°$. In this case the critical Mach number is not exceeded and an undisturbed flow can be expected. As a result, pure harmonic excitation produces a pressure response comprising only a first harmonic part. In the case of a higher angle of attack (Fig.17b), the critical Mach number is greatly exceeded. The resulting shock leads to a local separation of the flow, which in turn causes higher harmonic parts of the unsteady pressure. In the region of reattached flow, the higher harmonic parts vanish again. Fig.18a displays the unsteady pressure magnitude for the case of a very weak shock ($M = 0.74, \alpha = 0°$). Since no flow separation occurs, the higher harmonic parts are quite low, as expected. Raising the angle of attack up to just $\alpha = 1°$ causes the shock to be considerably more intense and the separation zone is extended. As anticipated, measurement points with higher harmonic parts of the unsteady pressure are found in this region. If the Mach number is raised to M = 0.78 (Fig.19a), the shock is even more intense and the flow separation extends to the trailing edge, though greatly weakened. The oblique shock at angle of attack $\alpha = 1°$ is not yet strong enough to cause the flow to separate. At $\alpha = 5°$, however, it causes a definite separation zone which extends over the normal shock and continues up to the trailing edge (Fig.19b). This figure shows that the higher harmonic parts constitute quite a large factor, particularly in this region of flow separation.

Comparison of measured and calculated results

Calculations were performed using an unsteady, time-linearized, potential-theoretical Transonic Method[3] in order to compare two wing configurations. This method takes the mean values and thus determines the first harmonics of the unsteady pressure distribution. For cases of small oscillation amplitudes, it is fully compatible with methods of the LTRAN[4] type but offers the advantage that mean values can be fitted or adapted to experimental investigations. In the two examples discussed here (high subsonic and local supersonic zones with moderately intense shock), the flow is attached. Small changes of the freestream Mach number and angle of attack show that the agreement between steady potential theory and experimentally determined mean values (Figures 20 and 21) is excellent. Nevertheless the theoretical unsteady results display noticeable deviations from the corresponding experimental values (Figs.20, 21):

a) Higher values for the real parts and lower values for the imaginary parts are obtained by theoretical calculation downstream from the supersonic zone (i.e. the suction tip on the upper side).

b) The considerably higher value of the theoretically obtained imaginary part in the upstream region is the most noteworthy discrepancy here.

Identical tendencies of the deviations between this theory and measurements in the same windtunnel were observed for the supercritical MBB A3 Profile.[5]

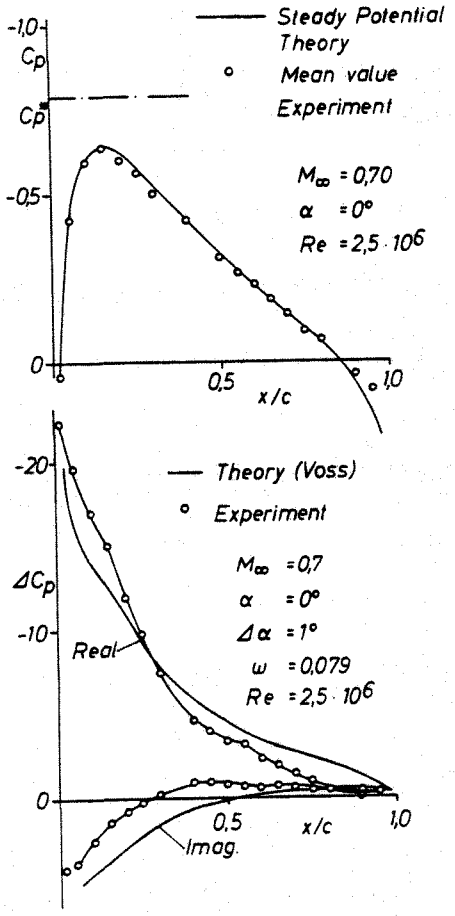

Figure 20: Comparison between theoretical and experimental mean and unsteady pressure distributions, $M_\infty = 0.70$.

On the other hand, the agreement between previous measurements taken in the NASA-Ames Transonic Windtunnel[6] (likewise with pitching oscillations) is quite good.[3] This fact coupled with the considerable differences found in the subcritical case indicate significant windtunnel influence, although the effects of unsteady friction are considered negligible.

It is of course a possibility that, although the mean pressure values are identical, the field values (and thus the spatial expansion of a supersonic zone perpendicular to the profile) differ for

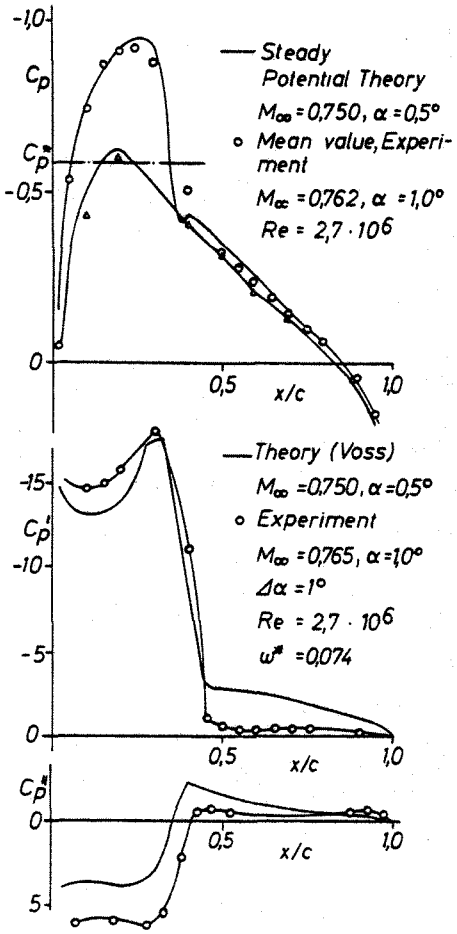

Figure 21: Comparison between theoretical and experimental mean and unsteady pressure distributions, M_∞ = 0.750 / 0.762.

theoretical and experimental results. Test calculations with artificial steady areas, where the extension of the supersonic region varies perpendicular to the profile, show for cases of unsteady pitch certain influences, however, that do not provide a quantitatively sufficient explanation for these discrepancies.

Conclusion

Steady, mean and unsteady aerodynamic data were measured on a rectangular wing with a theoretical NACA 0012 profile in two-dimensional flow. The wing was induced to perform pitch oscillations about its c/4-axis in order to produce the unsteady data. The purpose of the tests was to provide experimental data for the development and assessment of transonic analytical codes as well as to obtain results for flow with shock and profound separation, which are undesirable effects for passenger aircraft.

One definite result of this investigation is that both the Mach number and the angle of attack have a significant effect on the intensity and location of shock. The oscillation frequency influences mainly the phase relationship between pressure and motion, while the oscillation amplitude alters the value of the unsteady pressure, making it markedly nonlinear in the shock region at separated flow. The higher harmonic parts of the unsteady pressure occurring in this region as a result of harmonic oscillation cannot be overlooked, and are dependent on the intensity of the shock.

Knowledge of the nonlinear dependence of unsteady pressure on the oscillation amplitude in addition to the occurrence of higher harmonic parts of unsteady pressure deserve particular attention with regard to the development of a practicable theoretical model for flutter calculations without having to solve the Navier-Stokes equation immediately.

A comparison of theoretical values in the realm of nonseparated flow shows good agreement for the mean pressure values. Somewhat less satisfactory is the agreement between the unsteady pressure distributions peculiar to the region after shock, the main reason for which is most probably the influence of the windtunnel walls.

References

[1] Compendium of Unsteady Aerodynamic Measurements. AGARD Report No.702 (1982).

[2] Weitemeier, B. and Uerlings, P.: Ein vielkanaliges Hochgeschwindigkeitsdatenerfassungssystem zur Messung und Analyse zeitabhängiger Signale. DFVLR Report IB 232-83 J 04 (1984).

[3] Geissler, W., Voss, R.: Investigation of the Unsteady Airloads on Airfoils with Oscillating Control in Sub- and Transonic Flows. Proc.Int'l.Symp. on Aeroelasticity, DGLR Report 82-01 (1982) pp.65-80.

[4] Ballhaus, W.F., Goorjian, P.M.: Implicit Finite-Difference Computations of Unsteady Transonic Flows about Airfoils. AIAA Jour.15, No.12, (1977) pp.1728-1735.

[5] Triebstein, H., Voss, R.: Transonic Pressure Distributions on a Two-Dimensional 0012 and Supercritical MBB-A3 Profile Oscillating in Heave and Pitch. Proc. 59th AGARD-SMP Spec. Meeting "Transonic Unsteady Aerodynamics and Its Aeroelastic Applications" Sept.9-14, 1984 in Toulouse/France. (Yet to appear).

[6] Davis, S.S., Malcolm, G.N.: Experimental Unsteady Aerodynamics of Conventional and Supercritical Airfoils. NASA TM 81221, Aug. 1980.